NeuroImage 197 (2019) 167–176

Contents lists available at ScienceDirect

NeuroImage

journal homepage: www.elsevier.com/locate/neuroimage

Bottom-up sensory processing can induce negative BOLD responses and reduce functional connectivity in nodes of the default mode-like network in rats

Rukun Hinz *, Lore M. Peeters, Disha Shah, Stephan Missault, Michaël Belloy, Verdi Vanreusel, Meriam Malekzadeh, Marleen Verhoye, Annemie Van der Linden, Georgios A. Keliris **

Bio-Imaging Lab, University of Antwerp, Belgium

ARTICLE INFO

Keywords:
Resting-state functional MRI
Functional connectivity
Visual stimulation
Default mode network
Rats

ABSTRACT

The default mode network is a large-scale brain network that is active during rest and internally focused states and deactivates as well as desynchronizes during externally oriented (top-down) attention demanding cognitive tasks. However, it is not sufficiently understood if salient stimuli, able to trigger bottom-up attentional processes, could also result in similar reduction of activity and functional connectivity in the DMN. In this study, we investigated whether bottom-up sensory processing could influence the default mode-like network (DMLN) in rats. DMLN activity was examined using block-design visual functional magnetic resonance imaging (fMRI) while its synchronization was investigated by comparing functional connectivity during a resting versus a continuously stimulated brain state by unpredicted light flashes. We demonstrated that the BOLD response in DMLN regions was decreased during visual stimulus blocks and increased during blanks. Furthermore, decreased inter-network functional connectivity between the DMLN and visual networks as well as decreased intra-network functional connectivity within the DMLN was observed during the continuous visual stimulation. These results suggest that triggering of bottom-up attention mechanisms in sedated rats can lead to a cascade similar to top-down orienting of attention in humans and is able to deactivate and desynchronize the DMLN.

1. Introduction

The brain is a complex network consisting of functionally interconnected regions that dynamically communicate with each other. Part of these interactions can be observed non-invasively using resting-state functional magnetic resonance imaging (rsfMRI) (Damoiseaux et al., 2006; Salvador et al., 2005; van den Heuvel and Hulshoff Pol, 2010). This technique relies on the detection of low frequency fluctuations (0.01–0.2 Hz) in the blood oxygen level dependent (BOLD) signal while the subject is at rest, *i.e.* not performing any task. The coordinated fluctuations in the signals of anatomically separated regions have been shown to reflect intrinsic brain networks and evidence suggests that they correspond to spontaneous neuronal activity (Krishnan et al., 2018; Ma et al., 2016; Petridou et al., 2013). The regions that show temporally highly correlated activity are considered to be functionally connected and are referred to as resting-state networks (RSNs) (Friston, 2011).

Since its discovery, rsfMRI has been widely used in human research to study RSNs in the healthy brain as well as their alterations in neuropathologies (Greicius, 2008; Hull et al., 2017; Zhou et al., 2017). More recently, comparable RSNs have also been detected in rodents (Gozzi and Schwarz, 2016; Jonckers et al., 2011; C.P. Pawela et al., 2008a,b; Sierakowiak et al., 2015). This finding has been very important as it opened a new window of pre-clinical investigations in (genetic) animal models of disease that can be investigated with different modalities at multiple scales, providing additional information about the underlying mechanisms (Nestler and Hyman, 2010; Trancikova et al., 2011). In addition, pre-clinical rsfMRI shows great potential in identifying early biomarkers for multiple neuropathologies and can be used as an excellent theranostic tool (Bertero et al., 2018; Li et al., 2017; Shah et al., 2016, 2013). However, the translation and interpretation of RSNs between rodents and humans remains challenging, among other reasons, due to the differences in anatomy, physiology and the required use of anesthesia in rodents (Pan et al., 2015). It is therefore of utmost importance to investigate and improve our understanding of specific rodent RSNs that have been suggested to be homologous to RSNs in humans.

* Corresponding author. Bio-imaging lab, University of Antwerp, Campus Drie Eiken, Building Uc 1.17, Universiteitsplein 1, 2610, Wilrijk, Belgium.
** Corresponding author. Bio-imaging lab, University of Antwerp, Campus Drie Eiken, Building Uc 1.07, Universiteitsplein 1, 2610, Wilrijk, Belgium.
E-mail addresses: Rukun.Hinz@uantwerpen.be (R. Hinz), Georgios.Keliris@uantwerpen.be (G.A. Keliris).

https://doi.org/10.1016/j.neuroimage.2019.04.065
Received 15 February 2019; Received in revised form 23 April 2019; Accepted 24 April 2019
Available online 25 April 2019

Abbreviations

AC	Auditory cortex
BOLD	Blood oxygen level dependent
BVS	Blocked visual stimulation
Cg	Cingulate cortex
CVS	Continuous visual stimulation
DMLN	Default mode-like network
DMN	Default mode network
FC	Functional connectivity
fMRI	Functional magnetic resonance imaging
FOV	Field of view
FWE	Family wise error
GLM	General linear model
HRF	Hemodynamic response function
ICA	Independent component analysis
ISO	Isoflurane
LGN	Lateral geniculate nucleus
MD	Matrix dimensions
MED	Medetomidine
PtA	Parietal association cortex
ROI	Regions of interest
RS	Retrosplenial cortex
RSB	Resting-state baseline scan
rsfMRI	Resting-state functional magnetic resonance imaging
RSNs	Resting-state networks
SC	Superior colliculus
SS	Somatosensory barrel field cortex
ST	Slice thickness
TE	Echo time
TR	Repetition time
VC	Visual cortex

A RSN that has raised a lot of interest in humans is the default mode network (DMN), which has been shown to be most active during rest and internally focused tasks and less active during externally oriented attention demanding cognitive tasks (Greicius et al., 2003). Thus, it has been classified as a "task-negative network" and has been shown to alternate its activity with "task-positive networks" (Fox et al., 2005). The DMN is thought to play a fundamental role in self-referential thought, mind-wandering, internally-oriented cognition, and autobiographical memory (Lin et al., 2017). In humans, this network consists of regions in the anterior pre-frontal cortex, posterior cingulate cortex/retrosplenial cortex (precuneus), hippocampal formation, medial and lateral parietal regions (Buckner et al., 2008; Laird et al., 2009; Liska et al., 2015). A default mode-like network (DMLN) suggested to be homologous to the human DMN has also been identified in rodents (Lu et al., 2012; Stafford et al., 2014). This DMLN comprises comparable regions, *i.e.* orbital cortex, prelimbic cortex, cingulate cortex, temporal association cortex, auditory cortex, posterior parietal cortex and parietal association cortex, retrosplenial cortex and hippocampus. Furthermore, besides anatomical similarities, few studies could indicate functional similarities such as the higher activity of the DMLN during rest vs task and the anti-correlation relationship of the DMLN with the task positive network (Rohleder et al., 2016; Schwarz et al., 2013).

In recent years, multiple human studies have shown that functional connectivity (FC) within the DMN is decreased when subjects are in a higher attentive and cognitive brain state associated with performing an internally guided (top-down) attention-demanding task (Elton and Gao, 2015; Fransson, 2006; Gao et al., 2013; Marrelec and Fransson, 2011). It is thought that this internally guided attention to external sensory input can suppress other internal processes associated with the DMN, resulting in this network's inactivation and relative disconnection (Gao et al., 2013; Mayer et al., 2010). However, it is not yet sufficiently understood if attentional guidance by externally driven factors (bottom-up) could also result in similar reduction of activity and connectivity in the DMN. In humans, some studies suggested that the DMN is not deactivated by simple sensory processing (Greicius et al., 2003). It should be noted, however, that the stimulus design in these studies was simple and predictable and thus not expected to continuously drive bottom-up attention. Interestingly, a study using simple but unpredictable visual stimuli could dynamically activate attention network and DMN indicating their interaction during stimulus-driven processes of attention (Hahn et al., 2007).

Neurophysiological experiments in the past few years suggest that top-down and bottom-up processes share overlapping neural systems and in particular the employment of the prefrontal and parietal network (for a review see (Katsuki and Constantinidis, 2014)). We conjectured, that similarly to top-down, bottom-up attention triggering stimuli could also deactivate DMN and reduce its connectivity. To test this hypothesis, we performed fMRI experiments in sedated rats driven by randomized (unpredictable) continuous visual stimulation (CVS) and compared DMLN activity and connectivity with a resting-state baseline scan (RSB) and a blocked visual stimulation (BVS) design.

2. Material and methods

2.1. Animals and ethical statement

In this study, we used male Long Evans wild type rats (N = 12) of 4 months of age (Long Evans, Janvier). Rats were kept under a normal day/night cycle (12/12) with an average room temperature of 20–24 °C and 40% humidity. Furthermore, rats were group housed and had *ad libitum* access to standard rodent chow and water. One animal was excluded from the analysis due to the detection of unilateral ventricular enlargement. All procedures were performed in accordance with the European Directive 2010/63/EU on the protection of animals used for scientific purposes. The protocols were approved by the Committee on Animal Care and Use at the University of Antwerp, Belgium (permit number: 2015–50), and all efforts were made to minimize animal suffering.

2.2. Animal preparation and anesthesia

Rats were first anesthetized using 5% isoflurane for induction and 2% isoflurane for maintenance (IsoFlo, Abbott Illinois, USA) in a mixture of 70% N_2 and 30% O_2. Animals were head fixed in the scanner using bite- and ear-bars and ophthalmic ointment was applied to the eyes. As soon as the animal was fixed in the scanner, medetomidine sedation (Domitor, Pfizer, Karlsruhe, Germany) was administered via a subcutaneous bolus of 0.05 mg/kg and isoflurane concentration was decreased to 0% over a time period of 5 min. Continuous subcutaneous infusion of medetomidine sedation of 0.1 mg/kg.h was started 15 min post bolus injection. Functional MRI scans were acquired starting from 30 min post-bolus injection until 1h05 min post bolus injection. The physiological status of the animals was monitored throughout the entire imaging procedure. Respiratory rate was obtained from a pressure sensitive pad (MR-compatible Small Animal Monitoring and Gating system, SA Instruments, Inc.) with a sampling rate of 225 Hz. Body temperature was closely monitored using a rectal thermistor and was maintained between (37.0 ± 0.1 °C) using a feed-back controlled warm air heat system (MR-compatible Small Animal Heating System, SA Instruments, Inc.). Furthermore, blood oxygenation was recorded using a pulse oxygenation meter (MR-compatible Small Animal Monitoring and Gating system, SA Instruments, Inc.) with a sampling rate of 450 Hz. After imaging procedures, animals received a subcutaneous bolus injection of 0.1 mg/kg

atipamezole (Antisedan, Pfizer, Karlsruhe, Germany) to counteract the effects of medetomidine and were placed in a recovery box with infrared heating for post-scan monitoring until the animal was fully awake.

2.3. MRI

All rat anatomical and functional data are available online (central .xnat.org, project_ID: RAT_Bottom-up).

Imaging procedures were performed with Paravision 6.0 using a 9.4 T BioSpec MR system (Bruker, Germany) with an active decoupled rat quadrature surface coil (Rapid biomedical, Germany) and a 98 mm diameter quadrature volume resonator for transmission (Bruker, Germany). First, three orthogonal anatomical multi-slice Turbo RARE T2-weighted images (field of view (FOV): (30 × 30) mm^2, matrix dimensions (MD): [256 × 256], 12 slices, Slice thickness (ST): 0.9 mm, echo time (TE)/repetition time (TR): 33/2500 ms, RARE factor: 8) were acquired to allow reproducible flat skull positioning of coronal slices. Then, a coronal anatomical reference scan was acquired using a multi-slice Turbo RARE T2-weighted sequence (FOV: (30 × 30) mm^2, MD: [256 × 256], 12 slices, ST: 0.9 mm, TE/TR: 33/2500 ms, RARE factor: 8), covering the brain from 3.3 mm anterior to bregma to 7.5 mm posterior to bregma (suppl. figure 1). Next, a B_0 field map was acquired to assess field homogeneity, followed by local shimming in a rectangular volume of interest in the brain to correct for the measured inhomogeneities. The RSB scan had an identical geometry to the reference scan and was acquired using a T2*-weighted single shot echo planar imaging (EPI) sequence (FOV: (30 × 30) mm^2, MD: [128 × 98], 12 slices, ST: 0.9 mm, TE/TR: 18/2000 ms) resulting in a voxel dimension of (0.234 × 0.313 x 0.9) mm^3 and a total scan duration of 10 min (300 vol). Subsequently, random continuous light flickering (see section 2.4) was turned on and after 1 min the CVS scan was acquired using the same parameters as the RSB (300 vol). Last, a BVS data set was acquired using the same parameters and sequence (380 vol; Fig. 1A).

2.4. Visual stimulation

Visual stimulation with flickering light was presented using a white LED coupled to a fiber-optic cable, which was centrally placed in front of the animal's head. The LED light was controlled by a voltage-gated device to control the triggering of the LED light (ON-OFF) driven by a RZ2

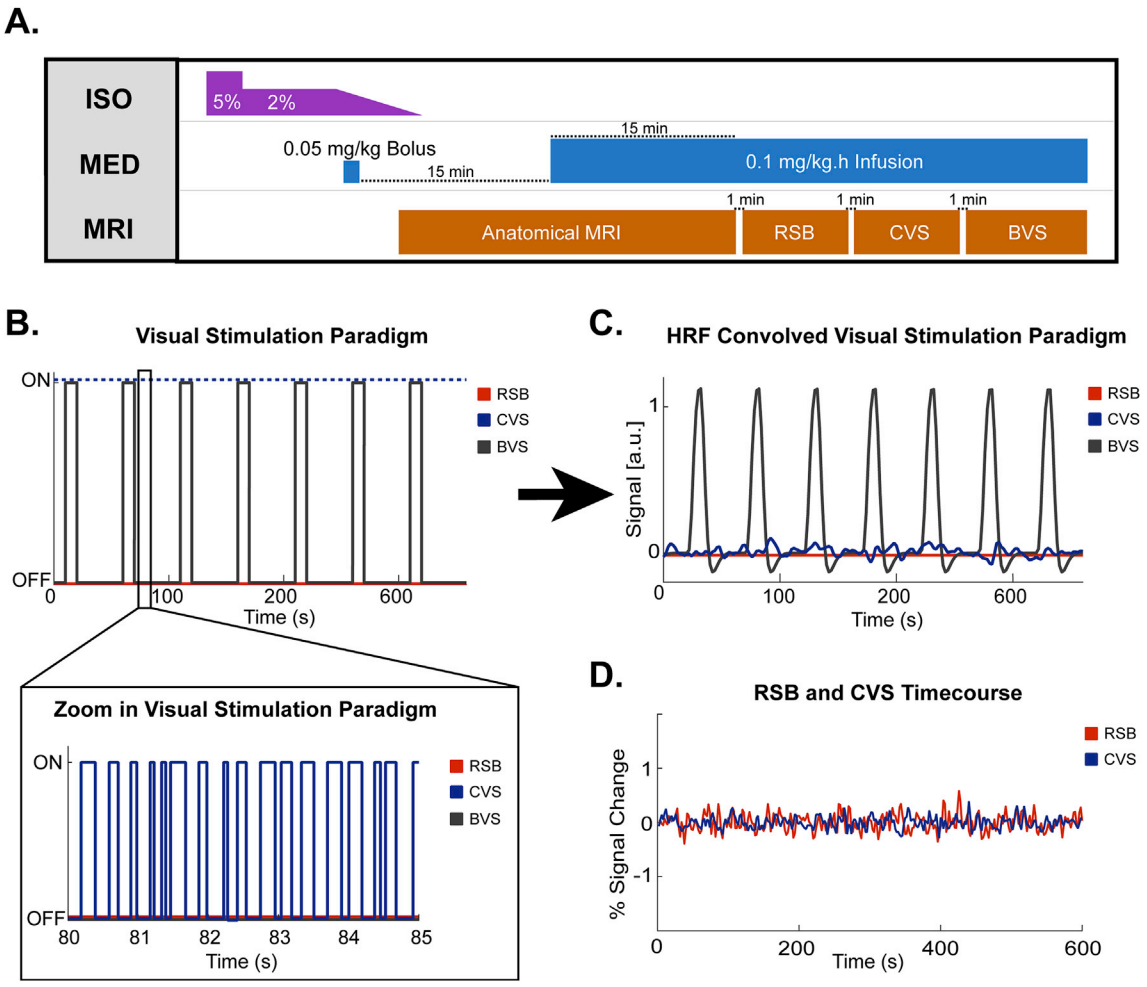

Fig. 1. Scanning protocol and visual stimulation paradigms. A. Scanning protocol. For handling procedures, animals were first anesthetized using 5% isoflurane (ISO) for induction followed by 2% ISO for maintenance. Once the animal is fixated in the scanner bed, a bolus of 0.05 mg/kg of medetomidine (MED) was administered and ISO anesthesia was gradually decreased to 0% ISO. After 15 min post bolus injection, a continuous infusion of 0.1 mg/kg.h MED was administered to the animal. For imaging procedures, first a set of anatomical Turbo RARE T2 scans were acquired and shimming procedures were performed. Next, 30 min post bolus injection a resting-state baseline (RSB) scan was acquired. Subsequently, continuous visual stimulation (CVS) paradigm was turned on and after 1 min the CVS scan was acquired. Lastly, after a recovery time of 1 min a block design visual stimulation (BVS) fMRI scan was acquired. B. Visual stimulation paradigm of RSB, CVS and BVS scan indicating when visual stimuli was turned on or off. C. Haemodynamic Response Function (HRF) convolved visual stimulation paradigm of RSB, CVS and BVS scan showing predicted BOLD signal response in arbitrary units (a.u.) from each condition. D. Example of acquired RSB and CVS normalized BOLD signal time course in the visual network.

BioAmp Processor (Tucker-Davis, Alachua). Stimulus timing and alignment to the MR imaging was achieved by TTL pulses sent by the scanner at the beginning of every volume of the fMRI scan.

2.4.1. Continuous visual stimulation

The CVS was used to induce a continuous visual sensory drive with randomization of light pulses to avoid sensory adaptation effects and to constantly trigger bottom-up attention mechanisms. This condition can be assumed to create a steady brain state similar to rest and thus could be analyzed the same way as the RSB scan (Fig. 1B–D). The CVS was initiated 1 min before the start of the acquisition to avoid the detection of the initial transient increase of brain activity, which occurs when the visual stimulation is turned on. The stimulation paradigm was controlled via Matlab code (MATLAB R2014a, The MathWorks Inc. Natick, MA, USA) using an USB to serial port connection (IC-232A, Rotronic) and consisted of continuous short pulses of light and inter-light intervals (both with a random duration between 50 and 250 ms) (Fig. 1B). Convolution of the CVS stimulus paradigm with the canonical hemodynamic response function (HRF) in SPM12 was performed in order to demonstrate that the expected signal fluctuations from CVS are negligible in comparison to those expected by the BVS paradigm (Fig. 1C).

2.4.2. Block design visual stimulation

To evoke BOLD responses from the visual system, fMRI scan was acquired during a block design paradigm with a visual stimulation frequency of 4 Hz, duty cycle 50% (125 ms ON/OFF), an initial OFF block of 10 s followed by 15 ON/OFF blocks of 10 s and 40 s respectively (Fig. 1B and C).

2.5. Breathing rate processing

Breathing rate pressure signals were analyzed to investigate the potential influence of visual stimulation on the animals' physiology. First, breathing rates were calculated for each volume by calculating the median period of the breathing cycle between the initial and the following volume and inverting this value to breaths per minute. For resting-state data, averaged breathing rate from the complete scans were compared between the RSB and CVS condition using a paired *t*-test ($p < 0.05$). For the BVS scans, averaged breathing rate over all visual stimulation blocks was compared 10 s before with 10 s during visual stimuli using a paired *t*-test.

2.6. MRI processing

All data processing was performed using SPM 12 software (Statistical Parametric Mapping, http://www.fil.ion.ucl.ac.uk), REST toolbox (REST1.7, http://resting-fmri.sourceforge.net) and GIFT toolbox (Group ICA of fMRI toolbox version 3.0a: http://icatb.sourceforge.net/).

Pre-processing consisted of realignment of the data towards the first image of each scan using a 6-parameter (rigid body) spatial transformation, normalization towards a study specific EPI template using a global 12-parameter affine transformation, followed by a non-linear transformation. Finally, data were smoothed in-plane using a Gaussian kernel with a full width at half maximum of twice the voxel size (0.458×0.626 mm). rsfMRI data were then further band pass filtered between 0.01 and 0.2 Hz using REST toolbox.

2.6.1. Functional connectivity

2.6.1.1. ICA components. To obtain the resting-state components from the rsfMRI data, an independent component analysis (ICA) was performed on RSB data. First, movement was regressed out of the data based on the estimators from the realignment procedure using the REST toolbox. Next, ICA was performed in GIFT using the Infomax algorithm with predefined number of 15 components as used previously (Jonckers et al., 2011). To identify the components in relation to previously reported RSNs (Gozzi and Schwarz, 2016; Jonckers et al., 2011; Lu et al., 2012; C.P. Pawela et al., 2008a,b; Sierakowiak et al., 2015), we first used a lenient threshold of z-score > 1 and discarded a minority of artefactual components (e.g. only edge of the brain) by careful visual inspection. Then, we adapted a more stringent threshold of z-score > 3 to visualize the core of the components and obtain masks for each network to use in further analysis.

2.6.1.2. ICA-based inter-component connectivity. To evaluate inter-component connectivity, network masks were used as regions of interest (ROI) in correlation-based analysis per subject. Pairwise Pearson correlation coefficients between the average BOLD time series of each ROI were calculated and Fisher z-transformed using an in-house Matlab program. Mean Fisher z-transformed inter-component correlation matrices were calculated for RSB and CVS conditions. Statistical analysis between conditions was performed using a repeated measures 2-way ANOVA ($p < 0.05$, Sidak correction for multiple comparisons). To calculate the FC between the DMLN and visual component, z-transformed correlation values of the cingulate-retrosplenial, hippocampal and temporal-prefrontal with visual component were averaged. Differences in correlation between the two conditions were then investigated using pairwise *t*-test ($p < 0.05$). To confirm our results, we delineated the DMLN (orbital cortex, prelimbic cortex, cingulate cortex, temporal association cortex, auditory cortex, posterior parietal cortex, parietal association cortex, retrosplenial cortex and hippocampus) and visual cortex based upon the Paxinos and Watson rat atlas. Pairwise Pearson correlation coefficients between the average BOLD time series of DMLN and visual cortex were calculated and Fisher z-transformed for both RSB and CVS condition. Statistical analysis between conditions was performed using a pairwise *t*-test ($p < 0.05$).

2.6.1.3. ROI-based intra- and inter-network connectivity. To investigate within and between network connectivity differences specific anatomically defined bilateral ROIs, selected on one slice in approximately the center of the ROI based upon the Paxinos and Watson rat atlas (6th edition) and taking into account the susceptibility artifacts of the GE-EPI image. ROIs were selected in the DMLN (cingulate cortex (Cg), retrosplenial cortex (RS), parietal association cortex (PtA), temporal association cortex (TeA)) as well as in the visual system (lateral geniculate nucleus (LGN), superior colliculus (SC), visual cortex (VC)) (suppl. figure 2). All ROIs consisted out of 32 voxels except TeA (20 voxels). Furthermore, a ROI in the primary somatosensory barrel field cortex (SS) was added as a control region. Pairwise Pearson correlation coefficients between the average BOLD time series of each ROI were calculated and Fisher z-transformed. Mean z-transformed ROI connectivity matrices were calculated for RSB and CVS conditions. To compare RSB and CVS condition, statistical analysis between conditions was performed using a repeated measures 2-way ANOVA ($p < 0.05$, Sidak correction for multiple comparisons).

2.6.1.4. Seed-based analysis. To investigate how the full-brain FC of the Cg is influenced by CVS, voxel wise seed-based analysis was performed. To this end, the mean time course of Cg was used as a predictor in a General linear model (GLM) and motion parameters were included as covariates. Afterwards, each subject's FC between Cg and DMLN or visual cortex was extracted by using the respective binarized masks derived from the ICA component and calculating the mean z-values within this mask for each individual subject. The DMLN network mask was constructed by the union of the cingulate-retrosplenial component mask, hippocampal component mask and temporal-prefrontal component mask. Statistical analysis to compare differences between the conditions was performed by means of a paired *t*-test ($p < 0.05$).

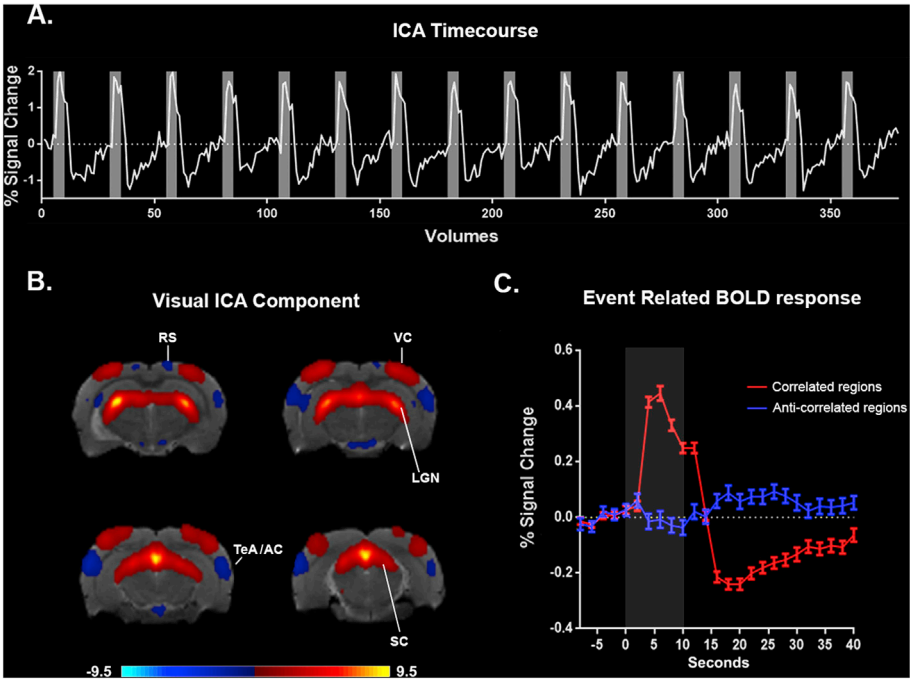

Fig. 2. Functional MRI ICA. A. ICA Time course. Time course from mean group visual ICA component with highest temporal correlation ($R^2 = 0.64$) with the visual stimulation paradigm (grey blocks). B. Visual ICA Component. Mean statistical group ICA map (z-score $-1<$ and >1) demonstrating areas which are correlated to the mean ICA component's time course involved in visual processing, i.e. visual cortex (VC), lateral geniculate nucleus (LGN) and superior colliculus (SC). Regions demonstrating a BOLD time course that is anti-correlated with the mean ICA component's time course, meaning higher BOLD signal during rest than during visual stimulation, were observed in DMLN regions i.e. temporal association cortex/auditory cortex (TeA/AC) and retrosplenial cortex (RS). C. Event related response of the regions correlating (Red) and anti-correlating (Blue) to the ICA component's time course. Grey block indicates visual stimulation period.

2.6.2. Block design fMRI

BVS data were processed using a group ICA approach using the GIFT toolbox with an Infomax algorithm and 15 predefined components. Group ICA analysis was chosen instead of the standard GLM to increase sensitivity towards detecting responding brain regions by not relying on predetermined BOLD HRF functions (Calhoun et al., 2009). The components temporal correlation with the visual stimulation paradigm was then calculated using R-square statistic in the GIFT toolbox. The component with highest temporal correlation with the visual stimulation paradigm were regarded as responding regions. Event related BOLD responses were extracted from a binary mask of responding regions, which are either correlated (z-score > 1) or anti-correlated (z-score < -1) with the ICA time course. To confirm our results, GLM analysis was performed for each subject using a canonical HRF function in SPM 12. The model was set to either detect a positive BOLD response during the stimulation period, to locate visual responding regions, or during the rest period, to detect regions which are more active during rest vs stimulation period i.e. DMLN activity. One sample *t*-test ($p < 0.001$, uncorrected for multiple comparisons) was performed to evaluate BVS group response.

3. Results

3.1. Block-design visual stimulation

To investigate whether activity in the DMLN of sedated rats is changing between visual sensory stimulation and rest periods, we analyzed the block-design fMRI experiment. To this end, we performed group-ICA analysis and sorted the components based on their temporal correlation with a HRF convolved visual stimulation paradigm. The component with the highest correlation ($R^2 = 0.64$) showed clear BOLD signal increases during the ON-blocks indicating a strong visual activation of multiple responding regions (Fig. 2A). The following highest correlating component ($R^2 = 0.19$) did not displayed similar BOLD signal increases. The mean group statistical ICA map (z-score > 1 and < -1) of the highest correlating component revealed that the activated regions were, as expected, areas involved in visual processing, *i.e.* the LGN, SC, VC (Fig. 2B). Event related analysis of all regions which are correlated with the ICA time course demonstrated that visual stimulation evoked a positive BOLD response as expected (Fig. 2C). Interestingly, we also observed regions such as the temporal association cortex/auditory cortex (TeA/AC) and RS, being anti-correlated to the ICA component's time course, indicating higher BOLD signal during rest vs stimulation (Fig. 2B). Event related analysis of anti-correlated regions with the ICA time course showed a subtle BOLD signal decrease during visual stimulation which rebounded and increased during blanks (Fig. 2C). To confirm our results, GLM modeling was applied and detected increased BOLD response during visual stimulation in LGN, SC and VC as well as increased BOLD response during blanks in TeA/AC (suppl. figure 3).

3.2. Resting-state vs continuous visual stimulation

3.2.1. Decreased intra- and inter-component connectivity during CVS

To identify potential changes in FC induced by our randomized continuous stimulation paradigm, we first performed group-ICA for the RSB condition and identified components which could represent commonly observed RSNs (Fig. 3). Functionally relevant components included three subcomponents of the DMLN: cingulate-retrosplenial component (with cingulate cortex, retrosplenial cortex and parietal association cortex), a hippocampal component (with subiculum, dentate gyrus, CA1 and CA3), and a temporal-prefrontal component (with orbitofrontal cortex, prelimbic cortex and temporal association cortex). Furthermore, ICA analysis detected components in the visual component, a caudate putamen, a primary and secondary somatosensory cortex, a barrel field cortex and a limbic system (including the amygdala and ventral striatum). Next, to evaluate intra- and inter-component connectivity, we threshold each ICA-component map (z-values > 3), extracted the time-courses and performed pairwise correlations for both the RSB and CVS conditions (Fig. 4). Statistical analysis comparing RSB and CVS condition using a repeated measures 2-way ANOVA (multiple comparison correction Sidak $p < 0.05$) detected a significantly decreased intra-DMLN component correlation in the CVS condition (*i.e* subcomponent cingulate-retrosplenial and temporal-prefrontal ($p < 0.001$)) as well as decreased inter-component correlations between DMLN subcomponent and the visual component (*i.e.* cingulate-retrosplenial with visual component ($p = 0.007$) and temporal-prefrontal with visual component ($p = 0.02$). Furthermore, this analysis was repeated using a less stringent ICA-component masks (z-value > 1) to extent all ICA components (suppl. figure 4). Similar analysis was also performed using DMLN and visual

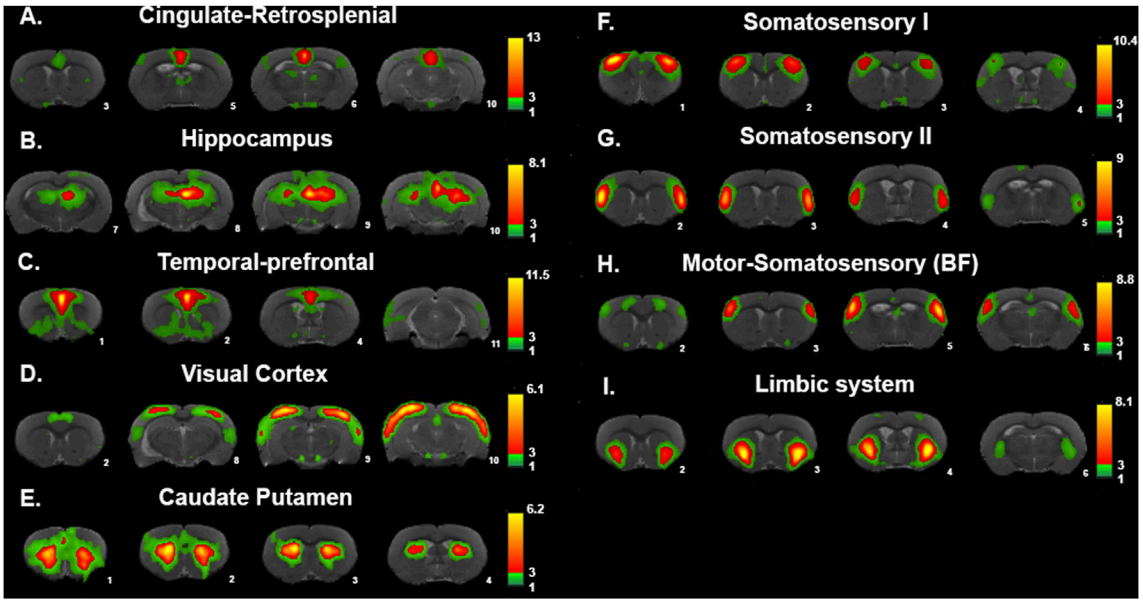

Fig. 3. ICA of Resting-State Baseline (RSB) condition. Mean group statistical ICA maps revealed nine functionally relevant components. A.-C. The DMLN in rats split up in three subcomponents i.e. A. Cingulate-Retrosplenial component (with cingulate, retrosplenial cortex and parietal association cortex), B. Hippocampal component (with subiculum, dentate gyrus, CA1 and CA3) and C. Temporal-prefrontal component (with orbito-frontal cortex, prelimbic cortex and temporal association cortex). D. Visual component (with visual and somatosensory cortex). E. Caudate Putamen component. F.-G. Primary and secondary somatosensory component. H. Barrel field component. I. Limbic component (with amygdala and ventral striatum). Color bar represents z-values.

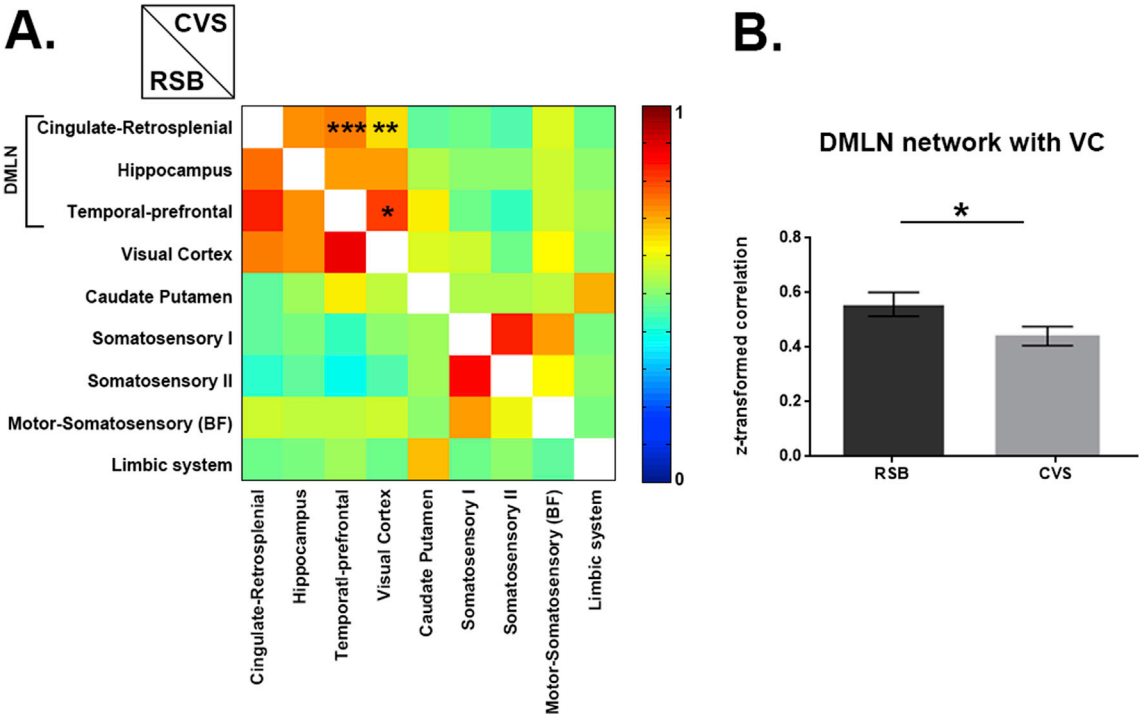

Fig. 4. Inter-component functional connectivity. A. Pairwise z-transformed Pearson correlation matrix of network components' (thresholded at z-value > 3) time courses of the resting-state baseline (RSB) (Bottom) and of the continuous visual stimulation (CVS) condition (Top). Stars indicate significant differences found between the two conditions with repeated measures 2-way ANOVA ($p < 0.05$, with Sidak multiple comparison correction). For CVS, significant decreased inter-conponent connectivity was found between subnetworks of the DMLN (i.e cingulate-retrosplenial component and temporal-prefrontal component) and between DMLN subcomponents and visual component. Color bar represents z-values. *$p < 0.05$, **$p < 0.005$, ***$p < 0.001$ B. Inter-component connectivity between DMLN and Visual component (average of connectivity between cingulate-retrosplenial and visual component, hippocampal and visual component, and temporal-prefrontal and visual component). Statistical analysis using a paired *t*-test detected a significant decreased inter-component connectivity in the CVS condition as compared to the RSB condition ($p < 0.05$).

cortex masks selected based upon the Paxinos and Watson atlas (suppl. figure 5). The results were qualitatively the same independent of the selected threshold.

Since CVS induced decreased inter-component correlation between the DMLN subcomponent and the visual component, we further assessed the pairwise correlation between specific ROIs of these components to zoom-in and better understand the sources of these decreases. ROIs in DMLN (*i.e.* Cg, RS, TeA and PtA) and visual system (*i.e.* LGN, SC and VC) were selected. In addition, we included the SS as a control area. Pairwise correlation between each ROI's averaged BOLD time course was performed and compared between RSB and CVS condition (Fig. 5). Statistical analysis using a repeated measures 2-way ANOVA (Sidak multiple comparisons correction $p < 0.05$) showed a decreased correlation between the DMLN ROIs *i.e.* Cg-RS ($p < 0.0001$), Cg-PtA ($p = 0.008$), RS-TeA ($p = 0.003$), RS-PtA ($p = 0.015$) and TeA-PtA ($p = 0.014$) as well as between DMLN and visual ROIs *i.e.* Cg-VC ($p < 0.0008$), RS-VC ($p = 0.0072$), TeA-VC ($p = 0.048$), and PtA-VC ($p = 0.0045$). None of these areas showed a significant change in correlation with the SS.

3.2.2. Voxel-based functional connectivity of cingulate cortex

The cingulate cortex, a major node of both DMLN in rodents as well as DMN in humans has been shown to change its activity during unpredictable stimuli (Hahn et al., 2007). Although the bottom-up randomized stimulation we have used does not capture any critical components of uncertainty used in top-down human studies, the randomized design avoids entrainment and habituation and has thus a higher bottom-up salience in comparison to periodic stimuli. To test if these stimuli would also influence the Cg, we selected this area for seed-based analysis. As demonstrated in the statistical FC maps (one sample *t*-test, $p < 0.001$, family wise error (FWE) corrected for multiple comparisons) presented in Fig. 6A, the Cg demonstrated wider brain connectivity during the RSB in comparison to the CVS condition. To further quantify this effect, we performed a paired *t*-test on the mean z-values within the DMLN or visual cortex. We found that CVS condition induced a decreased correlation between Cg and DMLN as well as between Cg and the visual component (Fig. 6B and C).

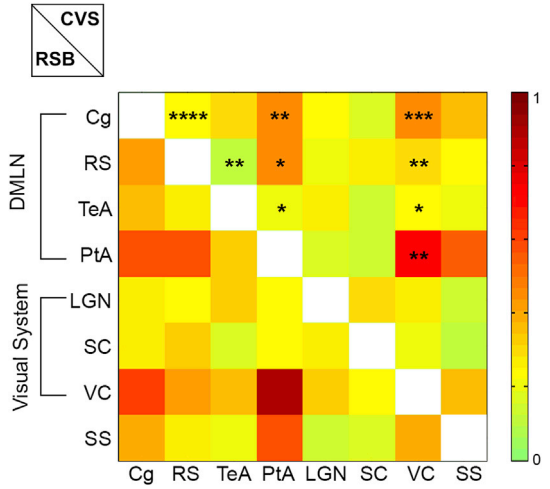

Fig. 5. ROI based analysis. A. Pairwise z-scored Pearson functional connectivity (FC) matrix between time courses of ROIs of the DMLN (i.e. cingulate cortex (Cg), retrosplenial cortex (RS), temporal association cortex (TeA) and parietal association cortex (PtA)), the visual system (i.e. lateral geniculate nucleus (LGN), superior colliculus (SC) and visual cortex (VC)) and the somatosensory barrel field cortex (SS) as a control region. Top half of the matrix represents FC of continuous visual stimulation (CVS) condition. Bottom half of the matrix represents FC of resting-state baseline (RSB) condition. Color bar represents z-values. Stars indicate significant differences found between the two conditions (diagonally symmetric positions) with repeated measures 2-way ANOVA ($p < 0.05$, with Sidak multiple comparison correction). Decreased FC was detected between DMLN ROIs i.e. Cg-RS, Cg-PtA, RS-TeA and RS-PtA as well as between DMLN and visual system ROIs i.e. Cg-VC, RS-VC, Tea-VC and PtA-VC. *$p < 0.05$, **$p < 0.005$, ***$p < 0.001$, ****$p < 0.0001$.

3.3. Unaltered breathing rate during visual stimulation

The pressure signal for breathing rate of the animals was recorded throughout the whole experiment and analyzed to assess potential changes on the general physiological state due to the visual stimulation. A paired *t*-test showed that there were no significant changes in breathing rate due to the visual stimulation ($p = 0.79$) (suppl. figure 6A). Breathing rate was further compared between RSB and CVS conditions using a paired *t*-test ($p < 0.05$). Likewise, CVS did not significantly alter the breathing rate ($p = 0.1$) (suppl. figure 6B).

4. Discussion

In the current study, we investigated the impact of visual stimulation on the DMLN activity and its FC in rats. We found that visual stimulation could deactivate nodes of the DMLN and could decrease FC within DMLN as well as across DMLN and visual networks.

4.1. Block design visual stimulation induces deactivation in DMLN regions

Block design visual stimulation was performed a) to identify the visually responsive areas and b) to investigate the influence of visual stimulation on the DMLN.

Similar to previous visual fMRI studies in rats, we detected activation of visual processing areas including LGN, SC, and VC (Chrisopher P. Pawela et al., 2008a,b; Van Camp et al., 2006). In addition to these activating regions, we detected regions that demonstrated a negative BOLD response during visual stimulation and displayed increased BOLD response during rest i.e. TeA/AC and RC. Interestingly, these areas have been shown to be nodes of the DMLN in rats (Lu et al., 2012). Negative BOLD responses in the DMN have been repetitively observed during top-down attention tasks in humans and monkeys (Arsenault et al., 2018; Greicius et al., 2003; Mantini et al., 2011). This could imply that bottom-up sensory processing could potentially activate similar pathways as top-down attention tasks resulting in negative BOLD responses of DMLN nodes. However, this finding seems in contrast to earlier human studies that did not detect significant reductions in DMN activity during passive sensory processing states that have low cognitive demand e.g. flashing checkerboard pattern presentation (Greicius et al., 2003). However, a number of important differences in our study could explain this discrepancy. Firstly, it should be noted that the effect we found in rats was very subtle. Thus, it is possible that similar effects could be present in humans but not sufficiently strong to be detected during awake conditions that are potentially compromised by additional processes. Previous studies directly demonstrated that the magnitude and extent of the suppression depends on the difficulty of the cognitive task (Leech et al., 2011; Mayer et al., 2010). As our study was performed in sedated rats, although not optimal for top-down cognitive processing, could be beneficial for identifying subtle bottom-up effects that could be otherwise hindered by additional variability induced by awake conditions. It is also noteworthy, that in this study we have used adolescent rats of 4 months of age. Even if in humans, DMN and top-down control from the prefrontal cortex continue to mature at this stage, in rats, the maturation age for these systems is not yet clearly defined (Hwang et al., 2010; Sato et al., 2014). To this end, Sierakowiak and colleagues in 2015, indicated homologies between rat (10–12 weeks) and adult human resting-state networks including the DMN (Sierakowiak et al., 2015), and Choi followed the maturation of DMN metabolic connectivity only up to 15 weeks referring to young adults (Choi et al., 2015). Importantly, the DMLN found in our study was comparable to the ones described in

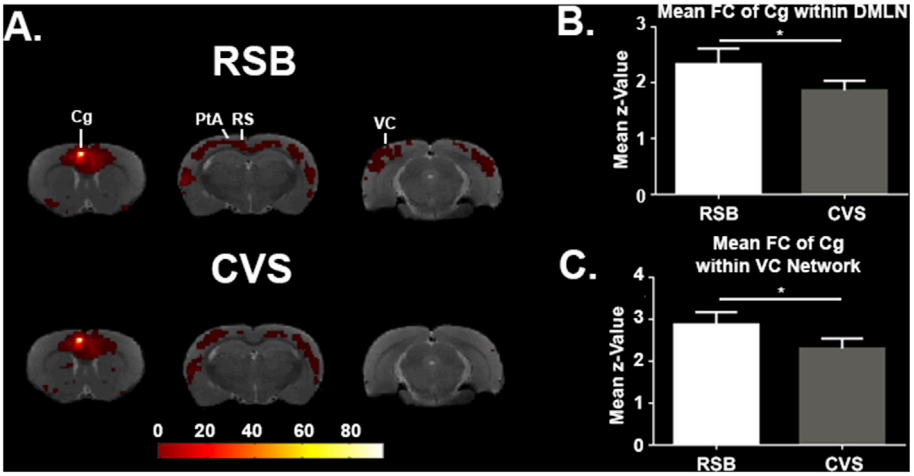

Fig. 6. Seed based analysis of functional connectivity with the cingulate cortex as seed region. A. Statistical maps of functional connectivity ($p < 0.05$ with family wise error correction (FWE) for multiple comparison correction) of the cingulate cortex (Cg) in the resting-state baseline (RSB) condition (Top) and continuous visual stimulation (CVS) condition (Bottom). Decreased FC in the parietal association cortex (PtA), retrosplenial cortex (RS) and visual cortex (VC) was observed in the CVS condition. Color bar represents t-values. High t-values indicate high functional connectivity with the seed B. Bar graph of the mean z-value with ±SEM within the default mode-like network. For each subject, mean z-values were extracted within the default mode-like network ICA mask. Results show that CVS significantly decreased connectivity of the Cg (paired *t*-test, $p < 0.05$) with the default mode-like network. C. Bar graph of the Mean z-value with ±SEM of all subjects within the Visual cortex (VC). For each subject, mean z-values were extracted within the VC component ICA mask. Results show that continuous visual stimulation (CVS) significantly decreased connectivity of the Cg (paired *t*-test, $p < 0.05$) with the VC.

previous studies in rats indicating that it can be considered by and large mature (Baliki et al., 2011; Gozzi and Schwarz, 2016; Jonckers et al., 2011; C.P. Pawela et al., 2008a,b; Sierakowiak et al., 2015). Moreover, evidence suggests that in humans top-down tasks are able to deactivate DMN in healthy adolescents (Chai et al., 2014; McCormick and Telzer, 2018). This could be indicative that this mechanism is also present in adolescent rats, but we note that in this study we have not used any top-down tasks but focused on bottom-up sensory stimulation instead. Given that bottom-up attention is thought to develop earlier (Amso and Johnson, 2006), we conjecture that using adolescence rats provides evidence that DMN suppression can be detected in this way at earlier stages. Further, given the suggestion that top-down and bottom-up attention share overlapping neural systems (Katsuki and Constantinidis, 2014), possible immaturity of top-down attention network could lead to a strengthened bottom-up response.

4.2. Continuous visual stimulation decreases inter- and intra-network FC of the DMLN

We explored the reorganization of functional networks during a visually stimulated brain state induced by CVS. The CVS paradigm was specifically developed to be salient and stochasticity was included to avoid habituation towards the stimulus. Firstly, ICA analysis was performed on the RSB data in order to identify components that resemble previously mentioned RSNs. These components showed strong bilateral connectivity and were similar to previously described RSNs in rats (Hutchison et al., 2010; Jonckers et al., 2011). We then investigated how the activity and connectivity within and across these components changed in the CVS condition.

By comparing FC between components in both conditions, we demonstrated that CVS decreased inter-network FC between DMLN subcomponents (cingulate-retrosplenial and temporal-prefrontal components (Lu et al., 2012)) and with the visual component. The observed decrease in inter-component connectivity during the CVS condition suggests an alteration in communication between the DMLN and the visual network. This finding could subserve the enhancement of local, input specific visual processing during CVS versus a higher inter-network communication during rest conditions.

Further, we performed ROI based analysis focusing on areas within the DMLN. This analysis demonstrated that intra-DMLN FC was also decreased. This included connections between multiple major nodes of the DMLN *i. e* Cg-RS, Cg-PtA, RS-PtA and RS-TeA. Similar to activity level decreases, connectivity decreases within human DMN were previously observed only with tasks involving higher cognitive load (Elton and Gao, 2015; Fransson, 2006; Gao et al., 2013; Marrelec and Fransson, 2011), while simple visual stimulation with a constantly flickering checkerboard pattern were not able to induce such deactivation (Di et al., 2015). Interestingly, the results observed in our study are more consistent with human data from subjects in a higher attentive and cognitive brain state.

5. Conclusion

In summary, we demonstrated that simple yet stochastic sensory stimulation in sedated rats could a) induce negative BOLD responses in certain nodes of the DMLN, and b) reduce intra- and inter-DMLN connectivity simulating similar results in humans performing task involving high cognitive and top-down attentional demand. We conjecture that the stochasticity of the stimulus, may play an important role in consistently and continuously driving bottom-up saliency mechanisms. Given that the bottom-up and top-down attentional systems share specific network components (Katsuki and Constantinidis, 2014), we hypothesize that both attention mechanisms are able to induce negative BOLD responses and reduce functional connectivity of the DMN. Our findings improve our understanding of the DMLN and bottom-up attention in animal models. In addition, they provide indications and new hypotheses to be tested in humans that are anesthetized or non-responsive as a result of trauma and or injury. However, to more explicitly demonstrate the link between attention systems and DMN activity and connectivity, more studies are required both in humans using stimuli specifically designed to continuously drive bottom-up attention, as well as in awake and behaving animals including more complicated cognitive tasks.

Acknowledgements

This research was supported by the fund of Scientific Research Flanders (grant agreement G048917N), Flagship ERA-NET (FLAG-ERA) FUSIMICE (grant agreement G.0D7651N) and by the doctoral grant BOF-DOCPRO 2015 from the University of Antwerp (granted to G.A.K).

Appendix A. Supplementary data

Supplementary data to this article can be found online at https://doi.

org/10.1016/j.neuroimage.2019.04.065.

References

Amso, D., Johnson, S.P., 2006. Learning by selection: visual search and object perception in young infants. Dev. Psychol. 42, 1236–1245. https://doi.org/10.1037/0012-1649.42.6.1236.

Arsenault, J.T., Caspari, X.N., Vandenberghe, X.R., Vanduffel, X.W., 2018. Attention Shifts Recruit the Monkey Default Mode Network, vol. 38, pp. 1202–1217. https://doi.org/10.1523/JNEUROSCI.1111-17.2017.

Baliki, M.N., Schnitzer, T.J., Bauer, W.R., Apkarian, A.V., 2011. Brain morphological signatures for chronic pain. PLoS One 6 e26010. https://doi.org/10.1371/journal.pone.0026010.

Bertero, A., Liska, A., Pagani, M., Parolisi, R., Masferrer, M.E., Gritti, M., Pedrazzoli, M., Galbusera, A., Sarica, A., Cerasa, A., Buffelli, A., Tonini, R., Buffo, A., Gross, C., Pasqualetti, M., Gozzi, A., 2018. Autism-associated 16p11.2 microdeletion impairs prefrontal functional connectivity in mouse and human. Brain 141, 2055–2065. https://doi.org/10.1093/brain/awy111.

Buckner, R.L., Andrews-Hanna, J.R., Schacter, D.L., 2008. The brain's default network: anatomy, function, and relevance to disease. Ann. N. Y. Acad. Sci. 1124, 1–38. https://doi.org/10.1196/annals.1440.011.

Calhoun, V.D., Lui, J., Adali, T., 2009. A review of group ICA for fMRI data and ICA for joint inference of imaging, genetic, and ERP data. Neuroimage 45, S163–S172. https://doi.org/10.1016/j.neuroimage.2008.10.057.A.

Chai, X.J., Ofen, N., Gabrieli, J.D.E., Whitfield-Gabrieli, S., 2014. Development of deactivation of the default-mode network during episodic memory formation. Neuroimage 84, 932–938. https://doi.org/10.1016/j.neuroimage.2013.09.032.

Choi, H., Choi, Y., Kim, K.W., Kang, H., Hwang, D.W., Kim, E.E., Chung, J.K., Lee, D.S., 2015. Maturation of metabolic connectivity of the adolescent rat brain. Elife 4, 1–12. https://doi.org/10.7554/eLife.11571.

Damoiseaux, J.S., Rombouts, S.A.R.B., Barkhof, F., Scheltens, P., Stam, C.J., Smith, S.M., Beckmann, C.F., 2006. Consistent resting-state networks across healthy subjects. Proc. Natl. Acad. Sci. Unit. States Am. 103, 13848–13853. https://doi.org/10.1073/pnas.0601417103.

Di, X., Fu, Z., Chan, S.C., Hung, Y.S., Biswal, B.B., Zhang, Z., 2015. Task-related functional connectivity dynamics in a block-designed visual experiment. Front. Hum. Neurosci. 9, 1–11. https://doi.org/10.3389/fnhum.2015.00543.

Elton, A., Gao, W., 2015. Task-positive functional connectivity of the default mode network transcends task domain. J. Cogn. Neurosci. 27, 2369–2381. https://doi.org/10.1162/jocn_a_00859.

Fox, M.D., Snyder, A.Z., Vincent, J.L., Corbetta, M., Van Essen, D.C., Raichle, M.E., 2005. The human brain is intrinsically organized into dynamic, anticorrelated functional networks. Proc. Natl. Acad. Sci. Unit. States Am. 102, 9673–9678. https://doi.org/10.1073/pnas.0504136102.

Fransson, P., 2006. How default is the default mode of brain function?. Further evidence from intrinsic BOLD signal fluctuations. Neuropsychologia 44, 2836–2845. https://doi.org/10.1016/j.neuropsychologia.2006.06.017.

Friston, K.J., 2011. Functional and effective connectivity: a review. Brain Connect. 1, 13–36. https://doi.org/10.1089/brain.2011.0008.

Gao, W., Gilmore, J.H., Alcauter, S., Lin, W., 2013. The dynamic reorganization of the default-mode network during a visual classification task. Front. Syst. Neurosci. 7, 1–13. https://doi.org/10.3389/fnsys.2013.00034.

Gozzi, A., Schwarz, A.J., 2016. Large-scale functional connectivity networks in the rodent brain. Neuroimage 127, 496–509. https://doi.org/10.1016/j.neuroimage.2015.12.017.

Greicius, M., 2008. Resting-state functional connectivity in neuropsychiatric disorders. Curr. Opin. Neurol. 24, 424–430. https://doi.org/10.1097/WCO.0b013e328306f2c5.

Greicius, M.D., Krasnow, B., Reiss, A.L., Menon, V., 2003. Functional connectivity in the resting brain: a network analysis of the default mode hypothesis. Proc. Natl. Acad. Sci. U. S. A 100, 253–258. https://doi.org/10.1073/pnas.0135058100.

Hahn, B., Ross, T.J., Stein, E.A., 2007. Cingulate activation increases dynamically with response speed under stimulus unpredictability. Cerebr. Cortex 17, 1664–1671. https://doi.org/10.1093/cercor/bhl075.Cingulate.

Hull, J.V., Jacokes, Z.J., Torgerson, C.M., Irimia, A., Van Horn, J.D., Aylward, E., Bernier, R., Bookheimer, S., Dapretto, M., Gaab, N., Geschwind, D., Jack, A., Nelson, C., Pelphrey, K., State, M., Ventola, P., Webb, S.J., 2017. Resting-state functional connectivity in autism spectrum disorders: a review. Front. Psychiatry 7. https://doi.org/10.3389/fpsyt.2016.00205.

Hutchison, R.M., Mirsattari, S.M., Jones, C.K., Gati, J.S., Leung, L.S., 2010. Functional networks in the anesthetized rat brain revealed by independent component analysis of resting-state fMRI, pp. 3398–3406. https://doi.org/10.1152/jn.00141.2010.

Hwang, K., Velanova, K., Luna, B., 2010. Strengthening of top-down frontal cognitive control networks underlying the development of inhibitory control: an fMRI effective connectivity study. J. Neurosci. 30, 15535–15545. https://doi.org/10.1523/JNEUROSCI.2825-10.2010.

Jonckers, E., Van Auderkerke, J., De Visscher, G., Van der Linden, A., Verhoye, M., 2011. Functional connectivity fMRI of the rodent brain: comparison of functional connectivity networks in rat and mouse. PLoS One 6, e18876. https://doi.org/10.1371/journal.pone.0018876.

Katsuki, F., Constantinidis, C., 2014. Bottom-up and top-down attention: different processes and overlapping neural systems. Neuroscientist 20, 509–521. https://doi.org/10.1177/1073858413514136.

Krishnan, G.P., González, O.C., Bazhenov, M., 2018. Origin of slow spontaneous resting-state neuronal fluctuations in brain networks. Proc. Natl. Acad. Sci. Unit. States Am. 201715841. https://doi.org/10.1073/pnas.1715841115.

Laird, A.R., Eickhoff, S.B., Li, K., Robin, D.A., Glahn, D.C., Fox, P.T., 2009. Investigating the functional heterogeneity of the default mode network using coordinate-based meta-analytic modeling. J. Neurosci. 29, 14496–14505. https://doi.org/10.1523/JNEUROSCI.4004-09.2009.

Leech, R., Kamourieh, S., Beckmann, C.F., Sharp, D.J., 2011. Fractionating the default mode network: distinct contributions of the ventral and dorsal posterior cingulate cortex to cognitive control. J. Neurosci. 31, 3217–3224. https://doi.org/10.1523/JNEUROSCI.5626-10.2011.

Li, Q., Li, G., Wu, D., Lu, H., Hou, Z., Ross, C.A., Yang, Y., Zhang, J., Duan, W., 2017. Resting-state functional MRI reveals altered brain connectivity and its correlation with motor dysfunction in a mouse model of Huntington's disease. Sci. Rep. 7, 1–9. https://doi.org/10.1038/s41598-017-17026-5.

Lin, P., Yang, Y., Gao, J., De Pisapia, N., Ge, S., Wang, X., Zuo, C.S., Jonathan Levitt, J., Niu, C., 2017. Dynamic default mode network across different brain states. Sci. Rep. 7, 1–13. https://doi.org/10.1038/srep46088.

Liska, A., Galbusera, A., Schwarz, A.J., Gozzi, A., 2015. Functional connectivity hubs of the mouse brain. Neuroimage 115, 281–291. https://doi.org/10.1016/j.neuroimage.2015.04.033.

Lu, H., Zou, Q., Gu, H., Raichle, M.E., Stein, E.A., Yang, Y., 2012. Rat brains also have a default mode network. Proc. Natl. Acad. Sci. Unit. States Am. 109, 3979–3984. https://doi.org/10.1073/pnas.1200506109.

Ma, Y., Shaik, M.A., Kozberg, M.G., Kim, S.H., Portes, J.P., Timerman, D., Hillman, E.M.C., 2016. Resting-state hemodynamics are spatiotemporally coupled to synchronized and symmetric neural activity in excitatory neurons. Proc. Natl. Acad. Sci. Unit. States Am. 113, E8463–E8471. https://doi.org/10.1073/pnas.1525369113.

Mantini, D., Gerits, A., Nelissen, K., Durand, J., Joly, O., 2011. Default mode of brain function in monkeys. J. Neurosci. 31, 12954–12962. https://doi.org/10.1523/JNEUROSCI.2318-11.2011.

Marrelec, G., Fransson, P., 2011. Assessing the influence of different ROI Selection Strategies on functional connectivity analyses of fMRI Data acquired during steady-state conditions. PLoS One 6, 1–14. https://doi.org/10.1371/journal.pone.0014788.

Mayer, J.S., Roebroeck, A., Maurer, K., Linden, D.E.J., 2010. Specialization in the default mode: task-induced brain deactivations dissociate between visual working memory and attention. Hum. Brain Mapp. 31, 126–139. https://doi.org/10.1002/hbm.20850.

McCormick, E.M., Telzer, E.H., 2018. Contributions of default mode network stability and deactivation to adolescent task engagement. Sci. Rep. 8, 18049. https://doi.org/10.1038/s41598-018-36269-4.

Nestler, E.J., Hyman, S.E., 2010. Animal models of neuropsychiatric disorders. Nat. Neurosci. 13, 1161–1169. https://doi.org/10.1038/nn.2647.

Pan, W.-J., Billings, J.C.W., Grooms, J.K., Shakil, S., Keilholz, S.D., 2015. Considerations for resting state functional MRI and functional connectivity studies in rodents. Front. Neurosci. 9, 20130152. https://doi.org/10.3389/fnins.2015.00269.

Pawela, C.P., Biswal, B.B., Cho, Y.R., Kao, D.S., Li, R., Jones, S.R., Schulte, M.L., Matloub, H.S., Hudetz, A.G., Hyde, J.S., 2008a. Resting-state functional connectivity of the rat brain. Magn. Reson. Med. 59, 1021–1029. https://doi.org/10.1002/mrm.21524.Resting-State.

Pawela, C.P., Hudetz, A.G., Ward, D.B., Schulte, M.L., Li, R., Kao, D.S., Mauck, M.C., Cho, Y.R., Neitz, J., James, H.S., 2008b. Modeling of region-specific fMRI BOLD neurovascular response functions in rat brain reveals residual differences that correlate with the differences in regional evoked potentials, 41, pp. 525–534. https://doi.org/10.1016/j.neuroimage.2008.02.022.Modeling.

Petridou, N., Gaudes, C.C., Dryden, I.L., Francis, S.T., Gowland, P.A., 2013. Periods of rest in fMRI contain individual spontaneous events which are related to slowly fluctuating spontaneous activity. Hum. Brain Mapp. 34, 1319–1329. https://doi.org/10.1002/hbm.21513.

Rohleder, C., Wiedermann, D., Neumaier, B., Drzezga, A., Timmermann, L., Graf, R., Leweke, F.M., Endepols, H., 2016. The functional networks of prepulse inhibition: neuronal connectivity analysis based on FDG-PET in awake and unrestrained rats. Front. Behav. Neurosci. 10, 1–10. https://doi.org/10.3389/fnbeh.2016.00148.

Salvador, R., Suckling, J., Coleman, M.R., Pickard, J.D., Menon, D., Bullmore, E., 2005. Neurophysiological architecture of functional magnetic resonance images of human brain. Cerebr. Cortex 15, 1332–2342. https://doi.org/10.1093/cercor/bhi016.

Sato, J.R., Salum, G.A., Gadelha, A., Picon, F.A., Pan, P.M., Vieira, G., Zugman, A., Hoexter, M.Q., Anés, M., Moura, L.M., Gomes Del'Aquilla, M.A., Amaro, E., McGuire, P., Crossley, N., Lacerda, A., Rohde, L.A., Miguel, E.C., Bressan, R.A., Jackowski, A.P., 2014. Age effects on the default mode and control networks in typically developing children. J. Psychiatr. Res. 58, 89–95. https://doi.org/10.1016/j.jpsychires.2014.07.004.

Schwarz, A.J., Gass, N., Sartorius, A., Risterucci, C., Spedding, M., Schenker, E., Meyer-Lindenberg, A., Weber-Fahr, W., 2013. Anti-correlated cortical networks of intrinsic connectivity in the rat brain. Brain Connect. 3, 503–511. https://doi.org/10.1089/brain.2013.0168.

Shah, D., Jonckers, E., Praet, J., Vanhoutte, G., Delgado Y Palacios, R., Bigot, C., D'Souza, D.V., Verhoye, M., Van der Linden, A., 2013. Resting state FMRI reveals diminished functional connectivity in a mouse model of amyloidosis. PLoS One 8 e84241. https://doi.org/10.1371/journal.pone.0084241.

Shah, D., Praet, J., Latif Hernandez, A., Höfling, C., Anckaerts, C., Bard, F., Morawski, M., Detrez, J.R., Prinsen, E., Villa, A., De Vos, W.H., Maggi, A., D'Hooge, R., Balschun, D., Rossner, S., Verhoye, M., Van der Linden, A., 2016. Early pathologic amyloid induces hypersynchrony of BOLD resting-state networks in transgenic mice and provides an early therapeutic window before amyloid plaque deposition. Alzheimer's Dementia 12, 964–976. https://doi.org/10.1016/j.jalz.2016.03.010.

Sierakowiak, A., Monnot, C., Aski, S.N., Uppman, M., Li, T.Q., Damberg, P., Brené, S., 2015. Default mode network, motor network, dorsal and ventral basal ganglia networks in the rat brain: comparison to human networks using resting state-fMRI. PLoS One 10, 1–20. https://doi.org/10.1371/journal.pone.0120345.

Stafford, J.M., Jarrett, B.R., Miranda-Dominguez, O., Mills, B.D., Cain, N., Mihalas, S., Lahvis, G.P., Lattal, K.M., Mitchell, S.H., David, S.V., Fryer, J.D., Nigg, J.T., Fair, D.A., 2014. Large-scale topology and the default mode network in the mouse connectome. Proc. Natl. Acad. Sci. Unit. States Am. 111, 18745–18750. https://doi.org/10.1073/pnas.1404346111.

Trancikova, A., Ramonet, D., Moore, D.J., 2011. Genetic Mouse Models of Neurodegenerative Diseases, 1st Ed, Progress in Molecular Biology and Translational Science. Elsevier Inc. https://doi.org/10.1016/B978-0-12-384878-9.00012-1.

Van Camp, N., Verhoye, M., De Zeeuw, C.I., Van der Linden, A., 2006. Light stimulus frequency dependence of activity in the rat visual system as studied with high-resolution BOLD fMRI. J. Neurophysiol. 95, 3164–3170. https://doi.org/10.1152/jn.00400.2005.

van den Heuvel, M.P., Hulshoff Pol, H.E., 2010. Exploring the brain network: a review on resting-state fMRI functional connectivity. Eur. Neuropsychopharmacol. 20, 519–534. https://doi.org/10.1016/j.euroneuro.2010.03.008.

Zhou, J., Liu, S., Ng, K.K., Wang, J., 2017. Applications of resting-state functional connectivity to neurodegenerative disease. Neuroimaging Clin. 27, 663–683. https://doi.org/10.1016/j.nic.2017.06.007.